Available online at www.sciencedirect.com
ScienceDirect
Diamond & Related Materials 16 (2007) 397–400
DIAMOND AND RELATED MATERIALS
www.elsevier.com/locate/diamond

Naturally formed epitaxial diamond crystals in rubies

Gyeong-Su Park [a,*], Sung Chul Bae [b], Steve Granick [b], Jang-Ho Lee [a], Sang-Duk Bae [c], Taekyung Kim [b], J.M. Zuo [b]

[a] *Analytical Engineering Center, Samsung Advanced Institute of Technology, San 14-1, Nong-Seo Ri, Ki-Hung Ueb, Yong-In Gun, Kyung-Ki Do, 449-900, Republic of Korea*
[b] *F Seitz Materials Research Laboratory, University of Illinois at Urbana–Champaign, 1304 West Green Street, Urbana, Illinois 61801, USA*
[c] *Gemological Institute of Korea, GemNuri Bd. 211, NakWon-Dong, JongNo-Gu, Seoul, Republic of Korea*

Received 17 January 2006; received in revised form 12 July 2006; accepted 21 August 2006
Available online 4 October 2006

Abstract

Materials inspired by nature comprise a running theme of modern science. Among the crystals that can be formed, diamond is perhaps most emblematic. In the conventional thinking, natural diamonds form only under high-pressure and high-temperature conditions. Here we show a new, natural form of diamond crystals of high quality that are epitaxial with their ruby substrate. Diamonds in rubies are rare; heteroepitaxial diamonds are twice as unexpected. Epitaxy suggests that the natural diamonds in the rubies were formed after ruby crystallization in a thermodynamically diamond stable region. This striking natural control over diamond epitaxy suggests a general strategy by which to form naturally-inspired, gem-quality crystals.

Keywords: Diamond; Epitaxy; Raman spectroscopy; Transmission electron microscopy

1. Introduction

Diamond-based electronics, optics and biosensors [1–3] require high-quality diamond crystals, such as epitaxially grown thin films. Heteroepitaxial diamond films on non-diamond substrates grown under low pressure and low temperature (diamond-metastable) conditions have attracted significant interest [4,5]. However, compared with natural diamonds, the synthetic diamond films by heteroepitaxy often show small crystals in sizes less than 0.5 μm [6–8] and the crystals suffer from many crystalline defects.

Ruby inclusions formed in diamonds were uncommonly reported [9]. As the singular case, diamonds were discovered in Vietnam ruby gems [10,11] as needle inclusions. The needle inclusions are large enough to be directly observed under an optical microscope (see the inset of Fig. 1a), and their dimension is about 0.6–1.4 mm long and 3–10 μm wide. Natural diamonds are commonly known to crystallize from volatile (C–H–O) rich fluids [12], or alkali-rich mantle fluids [13,14] at pressures of 5–6 GPa and temperatures in the range of 900–1400 °C [15]. This is well beyond ruby formation conditions (~0.2–1.05 GPa and 500–750 °C depending on geological locations) [16,17]. However, it is not reasonable to suppose that these diamonds were pre-formed in the needle inclusions and trapped before the crystallization of the ruby host, as natural diamond gem deposits are not known in the geologic area of Vietnam.

2. Experimental

To clarify the nature of the diamonds in the Vietnam ruby, we carefully characterized the diamond structure/morphology and the inclusion chemistry using transmission electron microscopy (TEM), confocal Raman microscopy, and optical microscopy. For TEM analysis, a thin cross-section of the needle inclusions was prepared using the focused ion beam (FIB) method. During the sample preparation, the positions of the inclusions in the ruby were accurately determined by laser marking with an optical microscope.

* Corresponding author. Fax: +82 31 280 9157.
E-mail address: sg8144.park@samsung.com (G.-S. Park).

0925-9635/$ - see front matter © 2006 Elsevier B.V. All rights reserved.
doi:10.1016/j.diamond.2006.08.031

3. Results and discussion

Fig. 1a shows a microscopy picture of the internal structure of the needle inclusion obtained at the enclosed rectangular region indicated in the inset. The width of the inclusion is about 3.0±0.5 μm. Four different minerals were found in the inclusion labeled M-1, M-2, M-3 and M-4. We note that mineral M-1 has a trapezoidal cross-section of ~1.0 μm sitting on the ruby host with a flat interface (as indicated by a black dotted line), which is unlike other interfaces in the inclusion. The crystal structures and chemical compositions of the four minerals were determined by high-resolution TEM (HRTEM), energy-dispersive X-ray spectrometry (EDS), and electron energy-loss spectroscopy (EELS); these data are summarized in Table 1 (see Supplementary data, Figs. S1, S2 and S3). The presence of Fe, Ni and Cr in the fluid inclusion is significant because both Fe and Ni are well known catalysts [18,19] for diamond growth and Cr is a good carbon solvent [19]. EELS analysis was performed to identify the bonding structure of the carbon mineral M-1 with the energy resolution of 0.8 eV. Fig. 1b compares one of the carbon K-edge electron energy-loss spectra obtained from mineral M-1 with that of a graphite particle. Unlike the alternative possibility of graphite, which has both π* peak (285 eV) and σ* peak, the observed pure σ* peak without π* states in the spectra obtained from mineral M-1 confirms carbon sp^3 bonding. This is characteristic of diamonds, as diamonds have only the σ* peak (290 eV) [20].

Table 1
Crystal structures and chemical compositions of the needle inclusion consisting of four minerals labeled M-1, M-2, M-3 and M-4

Minerals	Crystal structures	Chemical compositions (at.%)
Ruby	Single crystal	Al: 39.9, O: 59.9, Cr: <0.2
Mineral M-1	Single diamond crystal	C: 100
Mineral M-2	Single TiO_{1+x} crystal	Ti: 48.9, O: 51.1
Mineral M-3	Amorphous or nanocrystalline AlO_x	Al: 49.7, O: 50.2, Cr: <0.1
Mineral M-4	Fe_2O_3 nanocrystals + amorphous Fe–Cr–Ni–F oxide	Fe: 49.6, O: 32.2, Cr: 8.8, Ni: 6.3, F: 3.1

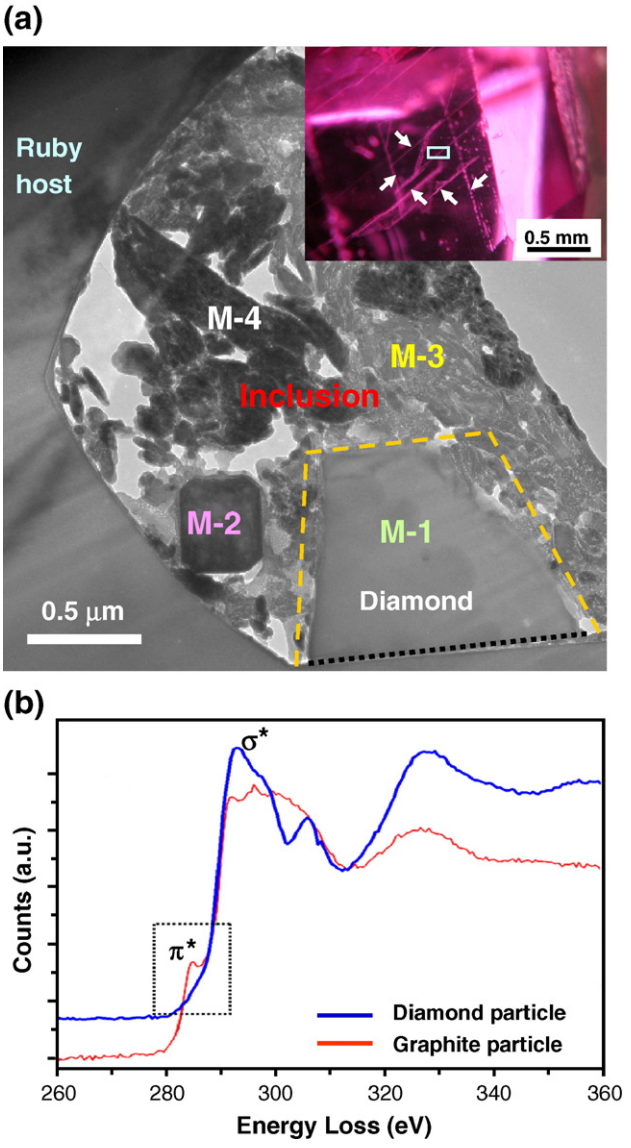

Fig. 1. Needle inclusions in a Vietnam ruby. The optical microscopy image in the inset shows the pinkish red Vietnam ruby and the needle inclusions (indicated by arrows). (a) A cross-sectional TEM image, which shows the internal structure of a needle inclusion in the Vietnam ruby. The inclusion consists of four minerals (M-1, M-2, M-3 and M-4). The black dotted line indicates the flat interface between the ruby host and the mineral particle M-1. (b) The carbon K-edge electron energy-loss spectra taken from the carbon mineral M-1. Compared to graphite, the carbon mineral M-1 shows only the σ* peak (290 eV) indicating sp^3 bonding and diamond structure.

The epitaxial relation of this diamond to the ruby substrate was another notable observation. Fig. 2a shows a TEM image of the flat interface between the ruby host and the diamond crystal. Ruby crystals have a hexagonal corundum structure. A selected area electron diffraction (SAED) pattern, taken from the ruby host, indicates that the ruby in the picture is oriented with the (0001) plane of the hexagonal structure parallel to the interface (Fig. 2b). Fig. 2c and d shows an SAED pattern and an HRTEM image, respectively, taken from the diamond particle. Both show a single crystal with the cubic diamond structure. Atomic distances, precisely measured by the SAED and nano-area electron diffraction (NED) pattern [21], also verify that the diamond has an *Fd3m* cubic structure. The crystallographic relation between the diamond crystal and the ruby matrix indicates that natural diamond grew in the {111} orientation (or (1$\bar{1}$1) according to the index of the diffraction pattern) on the ruby (0001) basal plane with an in-plane relationship of diamond [011]//ruby [10$\bar{1}$0]. It must be pointed out that this orientation relationship is exactly the same as for epitaxially grown synthetic diamonds on a sapphire substrate [22], which has the same crystal structure as the ruby. The (0001) plane of the ruby is hexagonal, which matches the symmetry of the diamond {111} lattice planes. The mismatch between the (0001) plane of the ruby and the {111} diamond planes is also small, 6% at ambient pressure and temperature. Low mismatch is a condition for heteroepitaxial growth.

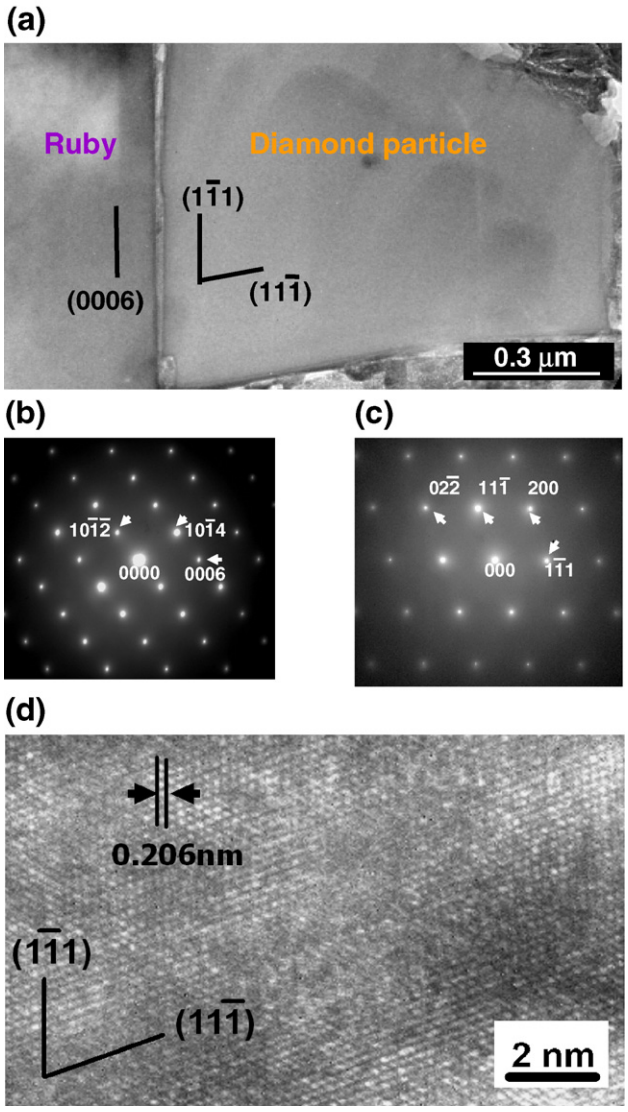

Fig. 2. TEM characterization of the diamond crystal M-1 formed on the ruby surface. (a) An enlarged TEM image of the flat interface between the ruby host and the diamond crystal M-1. The lines indicate the lattice planes of the ruby and diamond. The origin of the gap at the interface is most likely an artifact induced during the TEM sample preparation. (b) and (c) SAED patterns taken from the ruby host and the diamond particle shown in (a). The ruby is oriented with the (0001) plane parallel to the interface. (d) An HRTEM image of the diamond crystal. Both the SAED patterns and the HRTEM image show that the single crystal structure of the cubic diamond particle grows in the (1$\bar{1}$1) orientation on the ruby (0001) basal plane.

In order to identify the three-dimensional (3-D) morphology of these diamonds, we used confocal Raman microscopy. First, an Ar^+ laser beam of 0.3 μm spot size was focused onto three positions along the needle inclusion and the ruby host for Raman spectroscopy (see the inset of Fig. 3a). The Raman spectra (Fig. 3a) unambiguously exhibit a sharp first-order diamond peak [23] at 1332±1 cm^{-1}, widely distributed in space, thus showing that the diamond crystals are distributed along the needle inclusion. The same Raman diamond peaks were also reproducibly detected in other needle inclusions. A Raman contour map (Fig. 3b) of the intensity of this diamond peak reveals a hexagonal faceted shape (~3.2 μm in a longitudinal size). Combining the cross-sectional TEM and the Raman mapping images, we show a schematic view of these epitaxially-grown natural diamond crystals (Fig. 3c).

Not only the diamond morphology but also the epitaxial relationship between the diamond and the ruby matrix strongly suggest that these diamond crystals were grown after ruby crystallization as a part of the needle inclusions. The nucleation mechanism of these diamonds at the flat ruby interface is unknown. However, some of conditions for the diamond formation can be provided. First, the composite needle inclusions with a variety of oxide and carbon minerals suggest that they are crystallized from trapped fluids, such as the needle inclusions in garnets [24], due to the fact that the chemistry of

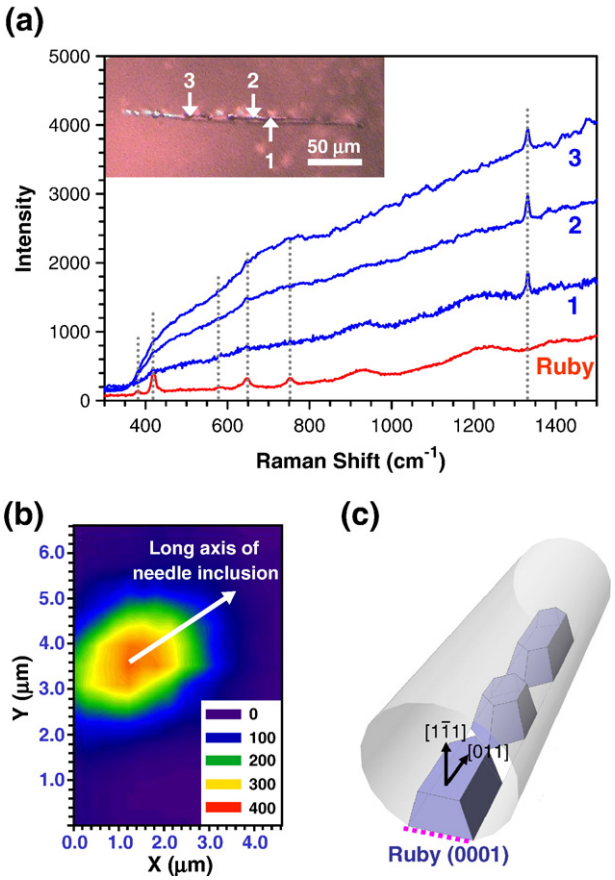

Fig. 3. Confocal Raman spectroscopy of the needle inclusion in a ruby. The optical microscope image showing the positions of Ar^+ laser beams focused on the needle inclusion is indicated in the inset. (a) Raman spectra obtained at three positions of the needle inclusion and the ruby host, using an excitation wavelength of 488 nm. The Raman spectra show sharp first-order diamond peaks at 1332±1 cm^{-1} and the five ruby characteristic peaks at 379±1 cm^{-1}, 417±1 cm^{-1}, 577±1 cm^{-1}, 646±1 cm^{-1}, and 751±1 cm^{-1}. (b) Raman contour map in the x–y plane of the intensity of the diamond (1332±1 cm^{-1}) obtained from the needle inclusion area 2 in the inset with a 0.3 μm spot. The diamond crystal has a hexagonal faceted shape. (c) Schematic view of natural diamond crystals epitaxially grown inside the needle inclusion in the Vietnam ruby. Hexagonal-shaped diamond crystals nucleated from the flat (0001) plane of the ruby and grew in the (1$\bar{1}$1) orientation with an in-plane arrangement. The diamond crystals were widely distributed along the needle inclusion corresponding to the diamond-[011] direction.

these minerals is impossible to be explained by a simple exsolution (unmixing of a solid solution) origin [25,26]. Secondly, it was recently reported the Vietnam ruby grew from a CO_2-rich and water-deficient fluid [11] at amphibolite metamorphic conditions. Thus, the carbon source for the diamond growth in the Vietnam ruby may be related to such a carbon-rich fluid because the carbon composition in the inclusion is only found in the diamond crystal M-1 (Table 1).

4. Conclusion

Looking to the future, this striking control over epitaxial diamond growth in nature suggests a more general strategy by which to form naturally-inspired, gem-quality crystals. Specifically, i) the heteroepitaxial crystal growth is perfectly orchestrated; crystal nucleation is promoted by smooth oxide surfaces and moreover the inclusion geometry provides alternative ruby surfaces, among which the nature selected (0001) surface, presumably owing to its symmetry and its match with diamond lattice. ii) Nature finds the needed chemistry; note that the needle inclusion studied here was rich in carbon and oxygen with impurities of Fe, Ni and Cr. Both Fe and Ni together with Cr are known solvent–catalysts for diamond growth in a thermodynamically diamond stable region. iii) On this basis, crystal growth proceeds optimally at this combination of temperature and pressure. Compared to synthetic diamond films grown by heteroepitaxy, the natural diamonds revealed here are exceptional in both size and crystal quality.

Acknowledgements

We thank Jung-Hyun Lim and E. Carol for their comments on the manuscript. We also appreciate the use of the facilities in the Center for Microanalysis of Materials, University of Illinois, which is partially supported by the U.S. Department of Energy (DOE). SCB, SG and JMZ acknowledge support by the DOE, Division of Materials Science.

Appendix A. Supplementary Information

Supplementary data associated with this article can be found, in the online version, at doi:10.1016/j.diamond.2006.08.031.

References

[1] S. Koizumi, K. Watanabe, M. Hasegawa, Science 292 (2001) 1899.
[2] E. Woerner, C. Wild, W. Muller-Sebert, p. Koidal. Diamond Relat. Mater. 10 (2001) 557.
[3] A. Härtl, E. Schmich, J.A. Garrido, J. Hernando, S.C.R. Catharino, S. Walter, P. Feulner, A. Kromka, D. Steinmüller, M. Stutzmann. Nat. Mater. 3 (2004) 736.
[4] B. Golding, C. Bednarski-Meinke, Z. Dai, Diamond Relat. Mater. 13 (2004) 545.
[5] F.P. Bundy, H.P. Bovenkerk, H.M. Strong, R.H. Wentorf, J. Chem. Phys. 35 (1961) 383.
[6] W.J. Zhang, X.S. Sun, H.Y. Peng, N. Wang, C.S. Lee, I. Bello, S.T. Lee, Phys. Rev., B 61 (2000) 5579.
[7] T. Tachibana, Y. Yokota, K. Miyata, T. Onishi, K. Kobashi, M. Tarutani, Y. Takai, R. Shimizu, Y. Shintani, Phys. Rev., B 56 (1997) 15967.
[8] A.A. Morish, P.E. Pehrsson, Appl. Phys. Lett. 59 (1991) 417.
[9] G.R. Watt, J.W. Harris, B. Harte, S.R. Boyd, Mineral. Mag. 58 (2004) 490.
[10] N.Q. Dao, V.X. Quang, N.Q. Huy, J.P. Silvestre, C.R. Acad, Sci. Paris 322 (1996) 515.
[11] G. Giuliani, J. Dubessy, D. Banks, H.Q. Vinh, T. Lhomme, J. Pironon, V. Garnier, P.T. Trinh, P.V. Long, D. Ohnenstetter, D. Schwarz, Chem. Geol. 194 (2003) 167.
[12] J.D. Blundy, J.P. Brodholt, B.J. Wood, Nature 349 (1991) 321.
[13] G.O. Bulanova, W.L. Griffin, C.G. Ryan, Mineral. Mag. 62 (1998) 409.
[14] O. Navon, I.D. Hutcheon, G.R. Rossman, G.J. Wasserburg, Nature 335 (1988) 784.
[15] S.E. Haggerty, Nature 320 (1986) 34.
[16] A. Peretti, J. Mullis, F. Mouawad, J. Gemmol. 25 (1996) 3.
[17] A. Mercier, P. Debat, J.M. Saul, Ore Geol. Rev. 14 (1999) 83.
[18] F.P. Bundy, Nature 241 (1973) 116.
[19] J.E. Field, The Properties of Diamond, Academic Press, New York, 1979.
[20] D.A. Muller, Y. Tzou, R. Raj, J. Silcox, Nature 366 (1993) 725.
[21] J.M. Zuo, M. Gao, J. Tao, B.Q. Li, R. Twesten, I. Petrov, Microsc. Res. Tech. 64 (2004) 347.
[22] M. Yoshimoto, K. Yoshida, H. Maruta, Y. Hishitani, H. Koinuma, S. Nishio, M. Kakihana, T. Tachibana, Nature 399 (1999) 340.
[23] A.V. Palnichenko, A.M. Jonas, J.C. Charlier, A.S. Aronin, J.P. Issi, Nature 402 (1999) 162.
[24] L. Wang, E.J. Essene, Y. Zhang, Contrib. Mineral. Petrol. 135 (1999) 164.
[25] L. Franz, R. Wirth, Contrib. Mineral. Petrol. 140 (2000) 283.
[26] J.S. White, Am. Miner. 64 (1979) 1300.